

m2sv: A Scalable Benchmark for Map-to-Street-View Spatial Reasoning

Yosub Shin¹ Michael Buriek^{1,2} Igor Molybog¹

Abstract

Vision–language models (VLMs) achieve strong performance on many multimodal benchmarks but remain brittle on spatial reasoning tasks that require aligning abstract overhead representations with egocentric views. We introduce **m2sv**, a scalable benchmark for map-to-street-view spatial reasoning that asks models to infer camera viewing direction by aligning a north-up overhead map with a Street View image captured at the same real-world intersection. We release **m2sv-20k**, a geographically diverse benchmark with controlled ambiguity, along with **m2sv-sft-11k**, a curated set of structured reasoning traces for supervised fine-tuning.

Despite strong performance on existing multimodal benchmarks, the best evaluated VLM achieves only 65.2% accuracy on m2sv, far below the human baseline of 95%. While supervised fine-tuning and reinforcement learning yield consistent gains, cross-benchmark evaluations reveal limited transfer. Beyond aggregate accuracy, we systematically analyze *difficulty* in map-to-street-view reasoning using both structural signals and human effort, and conduct an extensive failure analysis of adapted open models. Our findings highlight persistent gaps in geometric alignment, evidence aggregation, and reasoning consistency, motivating future work on grounded spatial reasoning across viewpoints.

1. Introduction

Vision–language models have demonstrated impressive capabilities in object recognition, diagram understanding, and text-heavy multimodal reasoning. However, they continue to struggle with tasks that require consistent spatial grounding across viewpoints. In particular, aligning abstract overhead representations such as maps with egocentric, ground-level

imagery remains a fundamental challenge. This capability is essential for applications in navigation, robotics, and embodied assistants, yet is weakly represented in current evaluation benchmarks.

Most existing multimodal reasoning benchmarks emphasize synthetic diagrams, charts, or carefully curated visual puzzles where geometry is simplified or explicitly annotated. Real-world spatial reasoning is substantially harder: it requires coping with viewpoint changes, partial observability, temporal mismatch between data sources, and ambiguity arising from repeated or symmetric structures. As a result, current benchmarks may overestimate spatial competence by avoiding the alignment of disparate viewpoints. We reserve a deeper discussion of related work and background for Appendix A.

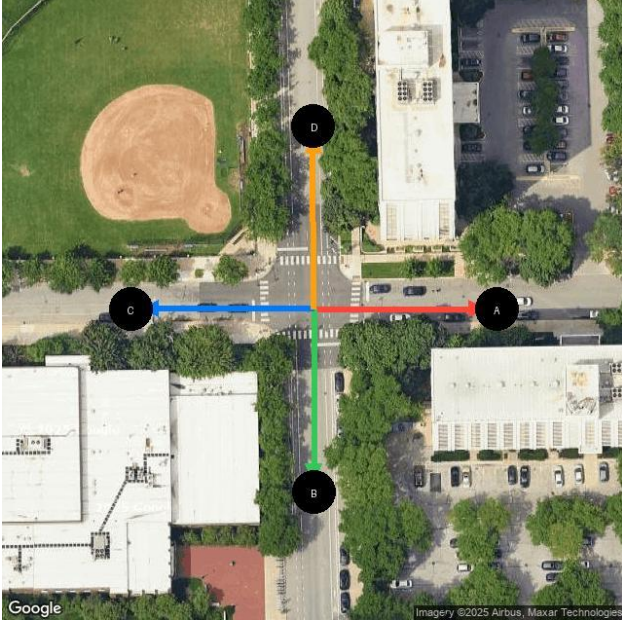
In this work, we introduce **m2sv** (map-to-street-view), a benchmark designed to isolate a core spatial reasoning primitive: inferring camera viewing direction by aligning a north-up overhead map with a Street View image captured at the same real-world intersection (Figure 1). Each example requires models to reason about road topology, intersection geometry, and stable landmarks, while ignoring transient or unreliable cues such as vehicles, lighting, or pedestrians. By grounding questions in real-world imagery and geometry, m2sv exposes failure modes that are largely hidden in synthetic or single-view tasks.

Beyond serving as a benchmark, m2sv enables a systematic study of *difficulty* in spatial reasoning. Because intersection geometry and candidate directions are known *a priori*, we can define scalable structural difficulty signals such as the number of candidate directions and angular symmetry. We complement these with human response-time measurements, allowing us to distinguish between structural ambiguity and human-perceived difficulty. This dual view reveals that even moderate geometric ambiguity induces sharp performance drops in models, while humans remain near ceiling.

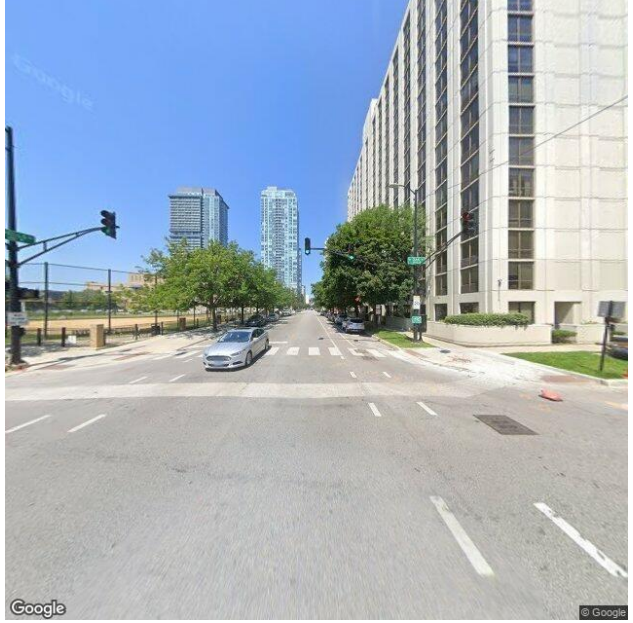
Finally, we perform an extensive failure analysis of our best adapted open model, going beyond aggregate accuracy to identify recurring breakdowns such as egocentric–allocentric confusion, symmetry traps, unreliable cue reliance, and internal reasoning inconsistencies.

Our contributions are:

¹University of Hawai‘i at Mānoa, Honolulu, HI, USA ²PwC, USA. Correspondence to: Yosub Shin <yosubs@hawaii.edu>.



(a) North-up overhead map with labeled candidate directions.



(b) Street View image captured at the same intersection.

Question

Which labeled direction on the map corresponds to the direction in which the street view photo was taken? Options: A, B, C, D.

Generated trace (Gemini-2.5-Pro)

Step 1: Analyze the street-view photo. The photo is taken from the center of an intersection, looking straight ahead. On the immediate right is a very tall, light-colored (white or beige) apartment or office building. It runs along the street from the corner onwards. On the immediate left is a fenced-off open area, which looks like a park or a sports field. There are trees lining the sidewalk. In the distance, further down the road, at least two prominent skyscrapers are visible. The road itself is a multi-lane street.

Step 2: Analyze the overhead map and evaluate each option. The camera is at the central intersection. Option A (looking East): To the right (south) is a large white building. To the left (north) is another large white building. This does not match the photo, which has a park/field on the left. Option B (looking South): To the right (west) is a large white building. To the left (east) is another large white building. This does not match the photo. Option C (looking West): To the right (north) is a large green area with a baseball field. To the left (south) is a large white building. This is the opposite of the street view (building on the right, park on the left). Option D (looking North): To the right (east) is a long, rectangular, light-colored building located right at the corner. To the left (west) is a large green area containing a baseball field. This arrangement perfectly matches the street-view photo.

Step 3: Conclude the comparison. Direction D is the only view from the intersection that has a large park/baseball field on the left and a tall, long building on the right. Final answer: \boxed{D}.

Ground truth

D

Figure 1. Illustrative m2sv example with paired images and a model-generated reasoning trace. The model correctly infers the viewing direction by aligning stable map geometry with the Street View image.

- A fully automated pipeline for constructing large-scale map-to-street-view spatial reasoning benchmarks, including image data sourcing, candidate response generation, and labeling tools.
- **m2sv-20k**, a geographically diverse benchmark with controlled ambiguity and statistically reliable evaluation, and **m2sv-sft-11k**, a curated set of structured reasoning traces for supervised fine-tuning.
- A systematic characterization of **difficulty in spatial reasoning**, combining structural signals (e.g., number

of candidate directions and angular symmetry) with human effort and model behavior (Section 6).

- An extensive evaluation and **failure mode analysis**, identifying recurring breakdowns such as egocentric–allocentric confusion, symmetry traps, unreliable cue reliance, and internal reasoning inconsistencies (Section 7).

2. Benchmark Design

Each m2sv example consists of two images: (1) a north-up overhead map centered at a real-world intersection, annotated with labeled directional rays, and (2) a Street View image captured near the same intersection and oriented along one of those rays. The task is to identify which labeled direction corresponds to the Street View camera orientation.

The number of candidate directions per example ranges from 2 to 7, with a median of 3 (mean: 3.24). Accordingly, the random-guess baseline is approximately 31.4%. Accuracy is measured over multiple-choice labels.

3. Dataset and Blueprint Pipeline

3.1. Blueprint specification

We decouple dataset specification from image rendering by releasing blueprint metadata that records intersection coordinates, candidate azimuths, correct labels, and Street View panorama identifiers. Images are rendered on demand using a standardized pipeline, enabling deterministic reconstruction of the dataset.

3.2. Sampling and filtering

Intersections are sampled from a seed list of major metropolitan areas worldwide to encourage broad geographic coverage. The sampling pipeline itself is city-agnostic and can be readily extended to additional regions by modifying the city list.

To control ambiguity and ensure fair evaluation, we apply several filtering criteria. Street View panoramas are restricted to within 5 m of the intersection center, resulting in a tightly controlled offset distribution (median: 2.05 m; 95th percentile: 4.51 m). We further enforce a minimum angular separation of 15° between candidate azimuths to exclude near-collinear road configurations that are difficult even for humans to disambiguate.

3.3. Dataset statistics

m2sv-20k contains 20,000 examples spanning 32 cities across multiple continents. Per-city caps prevent overrepresentation of dense urban areas. The number of candidate directions per example ranges from 2 to 7 (min: 2, max: 7, mean: 3.24, median: 3). Table 3 in the appendix reports additional statistics.

3.4. Reasoning traces

We curate **m2sv-sft-11k**, a subset of 11,000 examples annotated with structured reasoning traces generated by Gemini-2.5-Pro. Traces explicitly compare map geometry and Street View imagery and terminate in a boxed final answer. Fine-

Table 1. Zero-shot baseline performance on m2sv with 95% confidence intervals.

Model	N	Accuracy (%)
Gemini-3-Pro	1k	65.2 ± 3.0
GPT-5	1k	57.2 ± 3.1
Gemini-2.5-Pro	1k	47.2 ± 3.1
Qwen3-VL-8B-Instruct	1k	35.5 ± 3.0
Qwen3-VL-235B-A22B-Thinking	1k	42.7 ± 3.1
Random baseline	1k	31.4 ± 2.9
Human baseline	200	95.0 ± 3.0

tuning on all traces slightly underperformed, so we filter to correct traces only, yielding 4.4k examples total (4.37k train, 485 validation). These traces are used exclusively for supervised fine-tuning experiments.

4. Experimental Setup

We evaluate a range of proprietary and open-source VLMs using a standardized prompt that describes the task and instructs models to ignore transient visual elements. Accuracy and 95% confidence intervals are reported.

We fine-tune from Qwen3-VL-8B-Instruct using LoRA for both SFT and RL. SFT uses the filtered correct-trace subset (4.4k) and LoRA improves accuracy by 1.2% over full-parameter SFT. We train with LR 2e-4, cosine schedule with 0.03 warmup ratio, batch size 4, and early stopping at 2.3 epochs (max 4), using 1xH200 for about 2 hours. RL starts from the SFT checkpoint and uses LoRA with LR 2e-5, generation_batch_size 64, per_device_train_batch_size 16, and gradient_accumulation_steps 16, trained on 2xH200 for about 36 hours; we report results from the step-550 checkpoint.

5. Results

5.1. Zero-shot baselines and the human performance gap

We begin by establishing zero-shot baselines and the human performance ceiling on m2sv. Table 1 reports accuracy for a range of proprietary and open vision-language models evaluated without task-specific adaptation, alongside a random baseline and human performance measured on a 200-example subset.

Human accuracy reaches 95%, establishing a clear upper bound on task difficulty and confirming that m2sv is reliably solvable by people despite real-world visual noise and temporal mismatch. In contrast, even the strongest proprietary model (Gemini-3-Pro) falls more than 30 points below human performance, while most open models oper-

Table 2. Adaptation results on m2sv-20k (10k validation).

Model	Training	Accuracy (%)
Qwen3-VL-8B	Base	34.3 \pm 0.9
Qwen3-VL-8B	SFT	39.8 \pm 1.0
Qwen3-VL-8B	SFT+RL	43.9 \pm 1.0

ate only marginally above the random baseline. This large and consistent gap indicates that zero-shot pretrained VLMs lack robust mechanisms for aligning overhead maps with egocentric street-level views.

5.2. Adaptation baselines on m2sv

We next evaluate whether task-specific adaptation can mitigate this gap. Table 2 reports results for Qwen3-VL-8B under three training regimes: the base model, supervised fine-tuning (SFT) on m2sv reasoning traces, and reinforcement learning (RL) applied on top of SFT.

Supervised fine-tuning yields a consistent improvement over the base model, and reinforcement learning provides an additional gain of approximately four points. These results demonstrate that m2sv-specific supervision teaches useful task structure and improves decision consistency. However, even after SFT and RL, performance remains more than 50 points below the human ceiling, indicating that adaptation alone does not close the gap in spatial alignment capability.

5.3. Cross-benchmark transfer

To assess whether improvements on m2sv reflect more general spatial reasoning abilities, we evaluate m2sv-trained models on established multimodal benchmarks. Table 4 in the appendix reports performance on a subset of commonly used benchmarks for Qwen3-VL-8B variants.

Transfer results are mixed and do not show consistent improvements across benchmarks. Some metrics improve under SFT or SFT+RL, while others degrade or remain unchanged. This sensitivity suggests that gains on m2sv do not reliably translate into broader multimodal reasoning improvements, and may instead reflect benchmark-specific adaptations.

5.4. Asymmetric transfer with MindCube

To further probe transferability, we conduct a focused evaluation on the MindCube suite, which also targets spatial reasoning but differs in input structure and output format. Table 5 in the appendix reports performance under multiple prompting configurations for Qwen3-VL-8B variants.

m2sv-trained models occasionally outperform the base model on MindCube, but gains are highly sensitive to

prompting format and are largest in *direct answer* settings. When explicit reasoning traces are requested, the base model matches or exceeds the adapted variants. Conversely, models trained on MindCube perform near random on m2sv, indicating asymmetric and limited transfer.

Together, these results suggest that current fine-tuning pipelines induce benchmark-specific reasoning policies rather than transferable spatial representations, despite surface-level similarity between tasks.

6. Measuring Difficulty in Map-to-Street-View Reasoning

A central challenge in evaluating spatial reasoning is defining what makes an example *difficult*. In the map-to-street-view task, difficulty does not arise from a single factor but from an interaction between intersection geometry and fine-grained visual confusability across candidate directions. We therefore distinguish between two complementary notions of difficulty: *structural difficulty*, which is automatically measurable and scalable, and *human-perceived difficulty*, which reflects the cognitive effort required to resolve subtle spatial ambiguities.

Structural measures are attractive for large-scale dataset analysis and potential curriculum learning, but they are necessarily coarse. Human-perceived difficulty, while expensive to obtain, provides a diagnostic signal that captures visual and semantic factors beyond geometry. We analyze both to characterize where current vision–language models succeed and where they fail.

6.1. Structural difficulty signals

6.1.1. STRUCTURAL DIFFICULTY VIA NUMBER OF CANDIDATE DIRECTIONS

We analyze difficulty through a structural lens using the number of candidate directions (#options) provided in each question. This quantity is derived directly from intersection geometry and is available for every example without human annotation, making it a scalable proxy for geometric ambiguity and a natural signal for dataset filtering or curriculum learning.

A direct comparison of raw accuracy across different values of #options is confounded by varying chance levels (e.g., 0.5 for two options vs. 0.25 for four options). To account for this, we report *chance-normalized accuracy gain*, defined as $(a - c)/(1 - c)$, where a is model accuracy and $c = 1/K$ is the chance accuracy for K options. This normalization measures how much useful signal a model extracts beyond random guessing.

Figure 2 reports chance-normalized performance as a func-

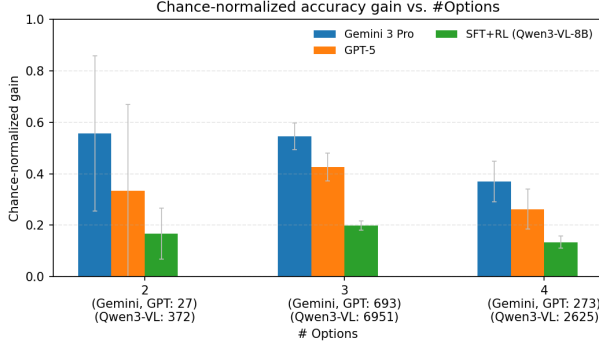


Figure 2. Chance-normalized accuracy vs. structural difficulty. Accuracy normalized by chance level as a function of the number of candidate directions (#options). Qwen3-VL-8B (SFT+RL) is evaluated on the full 10k validation set, while Gemini 3 Pro and GPT-5 are evaluated on a 1k subset. Three-option intersections yield the highest normalized gains across models, reflecting the benefit of geometric asymmetry. Error bars denote 95% binomial confidence intervals.

tion of the number of options (2, 3, and 4) for our best open model (Qwen3-VL-8B SFT+RL) evaluated on the full 10k validation set, and for two strong proprietary models evaluated on a 1k subset. This enables a statistically stable, large-scale analysis of structural difficulty.

Across all models, normalized performance does *not* degrade monotonically with the number of options. Instead, three-option intersections yield the highest normalized gains, outperforming both two- and four-option cases. This pattern is consistent across open and proprietary systems and reflects the role of geometric asymmetry: three-way intersections are often T-junctions with distinctive spatial layouts, whereas two- and four-way intersections are more likely to be symmetric and thus ambiguous.

These results demonstrate that the number of candidate directions alone is an incomplete measure of structural difficulty. Intersection cardinality interacts with geometric symmetry, and higher difficulty arises not simply from having more choices, but from the absence of asymmetry that can break directional ambiguity. This motivates the finer-grained structural and perceptual difficulty analyses that follow.

6.1.2. STRUCTURAL AMBIGUITY VIA ROAD-AZIMUTH SYMMETRY

The number of options captures how many candidate directions are present, but not how *interchangeable* those directions are. To refine the notion of structural difficulty, we introduce a road-azimuth symmetry measure based on the angular spacing between candidate directions. Intersections with evenly spaced azimuths (e.g., four-way junctions) are geometrically symmetric, while those with highly uneven

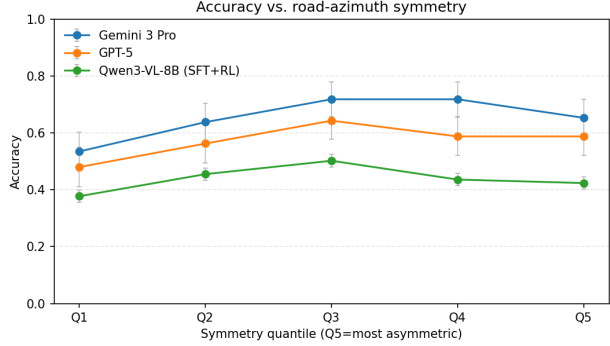


Figure 3. Accuracy vs. road-azimuth symmetry. Model accuracy as a function of azimuth symmetry quantiles (Q1 = most symmetric, Q5 = most asymmetric). Structural symmetry alone does not predict difficulty: accuracy peaks at intermediate symmetry levels and degrades in both highly symmetric and highly asymmetric regimes. Error bars denote 95% binomial confidence intervals.

spacing exhibit a dominant road direction and are structurally asymmetric.

Figure 3 shows model accuracy as a function of azimuth symmetry quantiles, with Q1 denoting the most symmetric and Q5 the most asymmetric examples. Across both open and proprietary models, accuracy does not decrease monotonically with symmetry. Instead, performance peaks at intermediate symmetry levels and declines slightly for both highly symmetric and highly asymmetric cases.

This non-monotonic trend indicates that azimuth symmetry is a necessary but insufficient explanation for difficulty. While structural asymmetry collapses the hypothesis space for humans—making these cases uniformly easy—it does not guarantee high model performance. Conversely, highly symmetric intersections enable difficult cases but do not make them uniformly hard.

6.2. Human effort as a difficulty proxy

Structural measures do not capture visual confusability between candidate directions, which often determines whether fine-grained spatial alignment is required. To probe these effects directly, we analyze difficulty as perceived by a human annotator, using response time as a proxy for cognitive effort.

During manual evaluation on a 200-example analysis subset, we record the elapsed time required for a human to answer each question. Figure 4 plots human response time as a function of azimuth symmetry. While highly asymmetric intersections are consistently easy for humans, symmetric intersections exhibit a wide spread of response times, ranging from trivially easy to extremely challenging. This demonstrates that structural symmetry defines an *upper bound* on difficulty but does not determine the realized difficulty of

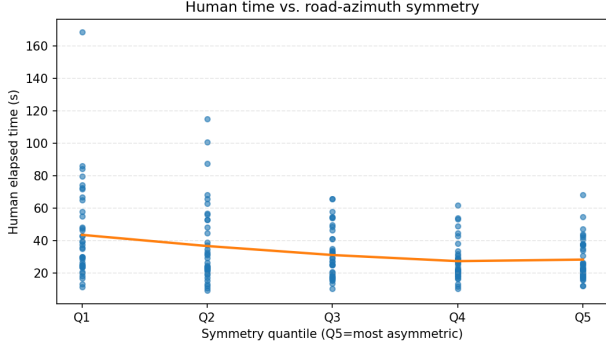


Figure 4. Human response time vs. road-azimuth symmetry. Each point denotes a single example from the 200-example analysis subset. Highly symmetric intersections exhibit a wide range of difficulty, while asymmetric intersections are uniformly easy for humans.

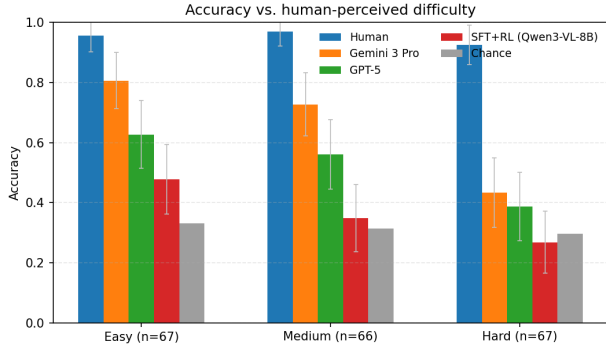


Figure 5. Accuracy vs. human-perceived difficulty. Accuracy as a function of difficulty defined by human response time. Examples are partitioned into Easy, Medium, and Hard buckets by response-time tertiles. Error bars indicate 95% binomial confidence intervals.

an example.

Finally, Figure 5 shows accuracy as a function of human-perceived difficulty, defined by tertiles of response time. Humans maintain near-ceiling performance across all buckets, with only a modest drop on the hardest examples, indicating that longer response times reflect increased effort rather than intrinsic ambiguity. In contrast, all evaluated models degrade sharply with increasing difficulty and approach chance-level performance on the hardest examples.

Taken together, these results suggest that model failures are driven not by geometry alone, but by an inability to exploit subtle, stable cues when visual ambiguity remains high. While structural asymmetry allows humans to shortcut the alignment process, current vision–language models do not reliably adapt their inference strategy to difficulty, motivating future work on difficulty-aware training and adaptive inference.

6.3. Model behavior vs. difficulty

We analyze how models modulate the length of their reasoning traces as a function of problem difficulty. As a proxy for difficulty, we use human annotation elapsed time, which correlates with structural ambiguity and symmetry. Trace length is measured as the approximate number of generated tokens in the model’s reasoning output.

Figure 6 reports average trace length across difficulty buckets (easy, medium, hard) for proprietary models and multiple variants of Qwen3-VL. We exclude GPT-5 from this analysis, as we observed that it does not reliably produce explicit reasoning traces and often responds with a direct answer only, making trace-length measurements inconsistent.

Both Gemini 3 Pro and Qwen3-VL-235B (Thinking) exhibit a clear monotonic increase in trace length with difficulty, indicating that these models expand their reasoning as ambiguity increases. Interestingly, the base Qwen3-VL-8B Instruct model shows a similar trend, despite its substantially lower accuracy, suggesting that it retains sensitivity to problem difficulty even when it lacks the capacity to resolve it reliably.

In contrast, both the supervised fine-tuned Qwen3-VL-8B (SFT) model and the Qwen3-VL-8B (SFT+RL) model produce nearly constant-length traces across difficulty levels. This indicates that the loss of difficulty-adaptive reasoning emerges during the supervised fine-tuning stage and is not recovered through reinforcement learning, even though overall accuracy improves. Together, these results suggest that current adaptation pipelines primarily optimize for earlier commitment to salient cues rather than preserving flexible, difficulty-aware deliberation.

Taken together, trace length modulation and task accuracy appear to be separable capabilities. Stronger proprietary models retain both difficulty awareness and effective multi-cue integration, while adapted open models achieve higher accuracy at the cost of reduced adaptive reasoning depth. This behavior aligns with the failure modes identified in Section 7, where adapted models often commit prematurely under symmetry or rely on a single dominant feature instead of escalating to finer-grained spatial evidence.

7. Failure Mode Analysis

To better understand why current vision–language models fail on m2sv despite strong zero-shot performance on other multimodal benchmarks, we conduct a qualitative failure analysis on a subset of challenging examples. Rather than attempting an exhaustive taxonomy, we focus on a small number of recurring failure patterns that consistently appear across models and difficulty regimes.

Importantly, these failures do not reflect fundamentally un-

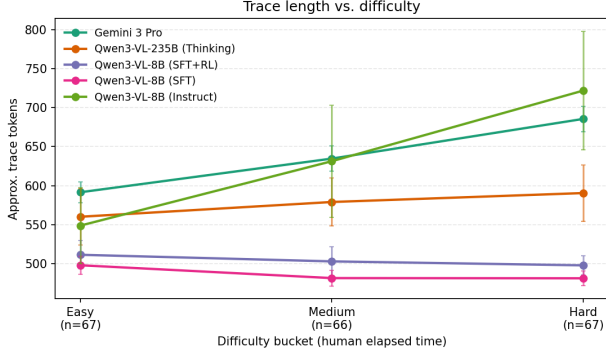


Figure 6. Reasoning trace length vs. difficulty. Average trace length (in tokens) as a function of difficulty, measured by human annotation elapsed time. Gemini 3 Pro and Qwen3-VL-235B (Thinking) increase trace length on harder examples, while Qwen3-VL-8B models adapted via SFT and SFT+RL produce near-constant-length traces despite higher accuracy. Error bars denote standard error of the mean.

solvable cases: human annotators are able to solve nearly all examples, often by investing additional effort and exploiting subtle but stable spatial cues. Model errors instead arise from brittle alignment strategies and inappropriate reliance on unreliable visual evidence.

Below, we summarize common failure modes observed in both open and proprietary models, illustrated with representative examples.

Egocentric–allocentric confusion (left–right inversion). Models frequently misinterpret the relationship between egocentric directions in the street-view image and allocentric directions on the overhead map. This often manifests as left–right inversions, where a correct identification of landmarks is followed by an incorrect mapping to map orientation, particularly at four-way intersections (Fig. 7a).

Over-reliance on unreliable cues. In many failures, models base eliminations on visually salient but unstable cues such as roof color, shadows, lighting conditions, or image blur. These cues are often weakly or not at all represented in overhead imagery and can vary substantially with capture time, leading to confident but incorrect conclusions (Fig. 7b).

Landmark misbinding. Models sometimes correctly identify salient landmarks in the overhead view but mis-associate them with the wrong candidate direction or parcel. For example, a swimming pool visible several houses away may be incorrectly attributed to the immediate intersection, leading to erroneous eliminations. This suggests limited precision in spatial binding between landmarks and their local context (Fig. 7c).

False landmark projection. In other cases, models introduce landmarks that are not present within the local intersection context, such as distant structures or perspective-induced artifacts. These projected landmarks are then treated as decisive evidence, despite lacking support in the overhead map, indicating weak control over spatial scope and relevance (Fig. 8d).

Failure to maintain a consistent spatial representation. In some failures, models do not maintain globally consistent spatial properties across options, treating shared structures as independent entities. This can manifest as assigning different road widths, lane counts, or landmark layouts to opposite headings of the same road, or contradicting earlier correct spatial descriptions during later reasoning. These errors suggest that models evaluate options in isolation rather than constructing and enforcing a coherent global spatial model (Fig. 8a).

Internal contradiction and state inconsistency. In some failures, models correctly identify spatial relationships or landmark configurations, but subsequently contradict themselves while reasoning or verbalizing the solution. These errors are characterized by internally inconsistent statements (e.g., asserting a correct left–right relation and then rejecting it), even though the underlying spatial alignment is correct. Unlike egocentric–allocentric confusion, these failures arise from an inability to maintain and consistently apply inferred spatial commitments across reasoning steps (Fig. 8b).

Symmetry traps and insufficient cue escalation. At symmetric or near-symmetric intersections, models often identify multiple plausible candidate directions but fail to escalate to finer-grained geometric cues—such as lane counts, road markings, curb geometry, or persistent vegetation—that would resolve the ambiguity. Instead, models rely on weak or unstable evidence and prematurely eliminate the correct option (Fig. 8c).

7.1. Implications.

Taken together, our analyses suggest that model failures on m2sv are not driven primarily by geometric complexity or lack of visual information, but by an inability to adapt inference strategies to the level of ambiguity present in an example. Structural asymmetry allows humans to shortcut reasoning on easy cases, while symmetric or visually confusable cases trigger deeper, more careful comparison. Current vision–language models, by contrast, exhibit relatively uniform reasoning behavior across difficulty regimes, leading to brittle decisions when subtle spatial cues are required.

This gap highlights an important limitation of current training and inference pipelines: models do not reliably escalate their reasoning depth or evidence aggregation in response



Ground truth: A, Prediction: C

Model trace (excerpt):

Looking from the center towards A, the road curves to the right. This contradicts the left curve seen in the photo.

Failure: Egocentric–allocentric left/right inversion: Overhead map shows a left curve, but model reasons as if it were a right curve.

(a) Egocentric–allocentric confusion (left–right inversion)



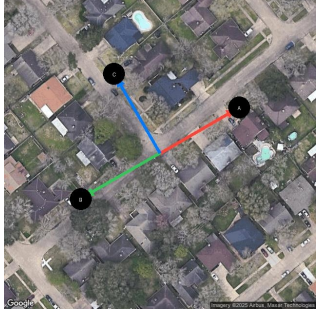
Ground truth: B, Prediction: D

Model trace (excerpt):

Looking south from the center, the buildings on both corners appear to have gray roofs. There is no prominent reddish-orange house on the left corner as seen in the photo. Therefore, B is incorrect.

Failure: The Street View angle of the roof is shallow, and the roof color is lighting-dependent. Humans would discount this cue.

(b) Over-reliance on unreliable visual cues



Ground truth: A, Prediction: B

Model trace (excerpt):

Facing direction A (east), we look down a relatively straight road. To the immediate left (north) of this view is a corner lot. The house on this corner has a large swimming pool in its backyard. This does not match the houses seen in the street view, which do not have prominent pools immediately adjacent to the road like this one does.

Failure: The corner house does not have a pool, but a pool exists two houses down. The model misattribution a nearby landmark to the wrong spatial anchor.

(c) Landmark misbinding

Figure 7. Representative qualitative failure modes on m2sv. Each row shows the same map–street-view pair with a different erroneous reasoning pattern exhibited by the model. From left to right: overhead map with candidate directions, corresponding street-view image, and an excerpt from the model’s reasoning trace highlighting the incorrect assumption. All examples are correctly solved by human annotators.

to increased difficulty. Addressing this limitation may require difficulty-aware training curricula, adaptive inference mechanisms, or explicit modeling of uncertainty in spatial alignment tasks.

8. Limitations

m2sv relies on the availability and coverage of commercial mapping services and reflects biases in their data collection. The benchmark focuses exclusively on public road intersections and does not include private or sensitive locations. The human evaluation is done with a limited number of volunteers.

9. Conclusion

m2sv provides a scalable benchmark for evaluating map-to-street-view spatial reasoning under real-world conditions. Despite advances in multimodal modeling, substantial gaps remain between VLMs and human performance. By isolating a core geometric alignment task and enabling large-scale evaluation, m2sv offers a useful diagnostic tool for future research on grounded spatial reasoning.

10. Acknowledgments

This work was supported by the National Science Foundation NRT-AI 2244574.

This work used cloud GPU resources at NCSA Delta cluster through allocation number CIS240027 from the Advanced Cyberinfrastructure Coordination Ecosystem: Services & Support (ACCESS) program, which is supported by National Science Foundation grants # 2138259, # 2138286, # 2138307, # 2137603, and # 2138296.

The technical support and advanced computing resources from University of Hawaii Information Technology Services – Research Cyberinfrastructure, funded in part by the National Science Foundation CC* awards # 2201428 and # 2232862 are gratefully acknowledged.

This material is based upon work supported by the National Science Foundation CISE Graduate Fellowships under Grant # 2313998. Any opinions, findings, and conclusions or recommendations expressed in this material are those of the author(s) and do not necessarily reflect the views of the National Science Foundation.

References

Berman, S. and Deng, J. Vlms have tunnel vision: Evaluating nonlocal visual reasoning in leading vlms. *arXiv preprint arXiv:2507.13361*, 2025.

Chen, H., Suhr, A., Misra, D., Snavely, N., and Artzi, Y. Touchdown: Natural language navigation and spatial reasoning in visual street environments. In *IEEE/CVF Conference on Computer Vision and Pattern Recognition (CVPR)*, pp. 12538–12547, 2019.

Glazer, E., Erdil, E., Besiroglu, T., Olsson, C. F., Denain, J.-S., Ho, A., Barnett, M., Sandler, R., Vrzala, M., and Sevilla, J. Frontiermath: A benchmark for evaluating advanced mathematical reasoning in ai. *arXiv preprint arXiv:2411.04872*, 2024.

Haas, L., Skreta, M., Alberti, S., and Finn, C. Pigeon: Predicting image geolocations. In *IEEE/CVF Conference on Computer Vision and Pattern Recognition (CVPR)*, pp. 12893–12902, 2024.

Hao, H., Han, M., Li, C., Li, Z. L., and Chang, X. Conav: Collaborative cross-modal reasoning for embodied navigation. *arXiv preprint arXiv:2505.16663*, 2025.

Huang, G., Zhou, Y., Zhao, L., and Gan, W. Cv-cities: Advancing cross-view geo-localization in global cities. *IEEE Journal of Selected Topics in Applied Earth Observations and Remote Sensing*, 2024.

Li, Z., Grossman, M., Qasemi, E., Kulkarni, M., Chen, M., and Chiang, Y.-Y. Mapqa: Open-domain geospatial question answering on map data. *arXiv preprint arXiv:2503.07871*, 2025.

Liu, L. and Li, H. Oriloc: Unlimited-fov and orientation-free cross-view geolocalization. *IEEE Transactions on Geoscience and Remote Sensing*, 2024. IEEE Document: 11037236.

Liu, Z., Sanyal, S., Lee, I., Du, Y., Gupta, R., Liu, Y., and Zhao, J. Self-contradictory reasoning evaluation and detection. In *Findings of the Association for Computational Linguistics: EMNLP 2024*, 2024.

Lu, P., Bansal, H., Xia, T., Liu, J., Li, C., Hajishirzi, H., Cheng, H., Chang, K.-W., Galley, M., and Gao, J. Mathvista: Evaluating mathematical reasoning of foundation models in visual contexts. In *International Conference on Learning Representations (ICLR)*, 2024. Oral presentation.

Mukhopadhyay, S., Rajgaria, A., Khatiwada, P., Shrivastava, M., Roth, D., and Gupta, V. Mapwise: Evaluating vision-language models for advanced map queries. In *North American Chapter of the Association for Computational Linguistics (NAACL)*, 2025.

Ott, S., Barbosa-Silva, A., Blagec, K., Brauner, J. M., and Samwald, M. Mapping global dynamics of benchmark creation and saturation in artificial intelligence. *Nature Communications*, 13(1):7593, 2022.

Shi, Y., Yu, X., Campbell, D., and Li, H. Where am i looking at? joint location and orientation estimation by cross-view matching. In *IEEE/CVF Conference on Computer Vision and Pattern Recognition (CVPR)*, pp. 4064–4072, 2020.

Shore, T., Mendez, O., and Hadfield, S. Spagbol: Spatial-graph-based orientated localisation. In *IEEE/CVF Winter Conference on Applications of Computer Vision (WACV)*, 2025.

Stanford HAI. Ai benchmarks hit saturation. <https://hai.stanford.edu/news/ai-benchmarks-hit-saturation>, 2024. Accessed: January 23, 2026.

Weyand, T., Kostrikov, I., and Philbin, J. Planet—photo geolocation with convolutional neural networks. In *European Conference on Computer Vision (ECCV)*, 2016.

Yin, B., Wang, Q., Zhang, P., Zhang, J., Wang, K., Wang, Z., Zhang, J., Chandrasegaran, K., Liu, H., Krishna, R., Xie, S., Li, M., Wu, J., and Fei-Fei, L. Spatial mental modeling from limited views. *arXiv preprint arXiv:2506.21458*, 2025.

Zhu, S., Yang, T., and Chen, C. Revisiting street-to-aerial view image geo-localization and orientation estimation. In *IEEE/CVF Winter Conference on Applications of Computer Vision (WACV)*, pp. 756–765, 2021a.

Zhu, S., Yang, T., and Chen, C. Vigor: Cross-view image geo-localization beyond one-to-one retrieval. In *IEEE/CVF Conference on Computer Vision and Pattern Recognition (CVPR)*, 2021b.

Zou, C., Guo, X., Yang, R., Zhang, J., Hu, B., and Zhang, H. Dynamath: A dynamic visual benchmark for evaluating mathematical reasoning robustness of vision language models. In *International Conference on Learning Representations (ICLR)*, 2025.

A. Background and Prior Work

This section situates the **m2sv** benchmark within the broader landscape of spatial AI, synthesizing research from spatial mental modeling, cross-view geo-localization, planetary-scale coordinate prediction, and map understanding.

A.1. Spatial Reasoning and Mental Modeling

The challenge of aligning allocentric and egocentric representations is a core problem in spatial AI. Recent work has focused on evaluating how Vision-Language Models (VLMs) form internal "cognitive maps" from limited views. The **MindCube** benchmark (Yin et al., 2025) introduced tasks such as perspective taking and mental rotation to probe this capability. Studies using MindCube revealed a significant "reasoning gap," where models excel at object recognition but fail to maintain consistent spatial models across rotational transformations. To address these failures, researchers proposed the "map-then-reason" paradigm, which uses explicit cognitive map generation to improve reasoning accuracy. The **m2sv** is designed to test very similar capabilities of the VLMs, but is based on a dataset that is much easier to scale from public data sources.

A.1.1. CHARACTERIZING VLM FAILURES IN SPATIAL REASONING

Recent diagnostics have highlighted several persistent failure modes in VLM spatial reasoning that align with our qualitative observations on **m2sv**. One fundamental deficiency is *left-right confusion* in egocentric directional tasks; as noted in (Hao et al., 2025), agent failures are often linked to an "insensitivity to directions (e.g., left/right)," which suggests a lack of robust internal coordinate systems even in models trained for embodied navigation. Beyond simple directionality, models frequently exhibit *internal logic contradictions*, where generated reasoning traces contain steps that directly conflict with the final answer or each other (Liu et al., 2024). This indicates that models may prioritize final-answer heuristics over logically consistent spatial modeling.

Furthermore, VLMs struggle with *cue weighting*, often prioritizing learned priors and background knowledge (e.g., standard road layouts) over the specific visual evidence presented in the images (Berman & Deng, 2025). This "tunnel vision" extends to *ambiguity handling*, where models fail to recognize when a visual scene is ambiguous and require saccadic search or detailed local investigation to resolve orientation. Instead, they often latch onto the first available cue without weighing its reliability against the global map geometry.

A.2. Cross-View Geo-Localization (CVGL)

The field of Cross-View Geo-Localization (CVGL) provides the technical context for matching ground-level imagery to overhead perspectives. However, existing benchmarks predominantly focus on *image-level retrieval* where the primary goal is to determine the geographic location (latitude/longitude) by matching street-view queries against a database of satellite reference patches. Datasets such as **CVUSA**, **CVACT**, and **CV-Cities** (Huang et al., 2024) are largely evaluated using Recall@K, a metric that rewards the ability to retrieve the correct image pair rather than the ability to reason about spatial orientation within that pair. Furthermore, many standard splits in these benchmarks simplify the task by using north-aligned panoramas, which allows models to normalize for orientation or bypass it entirely (Zhu et al., 2021a). Even more complex settings like **VIGOR** (Zhu et al., 2021b), which introduces spatial offsets, still operate within a black-box feature matching framework where low-level visual correlations (e.g., matching roof textures or vegetation patterns) often serve as a powerful shortcut for retrieval.

In contrast, **m2sv** shifts the focus from *global retrieval* to *local spatial reasoning*. By fixing the location at a specific intersection and providing multiple candidate orientations, **m2sv** isolates orientation as the primary reasoning bottleneck. It requires the model to perform a geometric alignment between the egocentric street view and the north-up overhead map, matching landmarks and road topology to deduce heading. This task is resistant to the retrieval shortcuts of traditional CVGL, as it demands an understanding of the 3D spatial relationship between views. While specialized sub-fields of CVGL have explored orientation estimation by retrieval systems (Shi et al., 2020; Liu & Li, 2024; Shore et al., 2025), **m2sv** provides a scalable and reasoning-focused benchmark that measures the gap in "directional intelligence" within vision-language models.

A.3. Planetary-Scale Coordinate Prediction

Beyond local matching, coordinate prediction models like **PIGEON** (Haas et al., 2024) and **PlaNet** (Weyand et al., 2016) attempt to estimate global coordinates from single images. While these models leverage semantic cues (e.g., vegetation, architectural styles) to predict location, they are often evaluated on geocell classification rather than fine-grained geometric reasoning. **PIGEON** achieved human-parity on GeoGuessr-style tasks, but its success relies heavily on regional attribute matching. In contrast, **m2sv** focuses on the *fine-grained spatial alignment* (pinpointing orientation at a known intersection) where AI dominance is not yet assured. Its purpose is to test out-of-distribution generalization to unseen spatial orientation problems.

Table 3. Summary statistics of the m2sv-20k dataset.

Statistic	Value
Number of examples	20,000
Number of cities	32
Candidate directions (median)	3
Street View distance (median)	2.05 m
Street View distance (95%)	4.51 m

Table 4. Cross-benchmark evaluation for Qwen3-VL-8B variants.

Model	MMMU	MME-Cog/Per	MMStar	Omni3D
Base	0.556	643 / 1721	0.604	0.388
SFT	0.574	501 / 1525	0.574	0.372
SFT+RL	0.563	550 / 1670	0.644	—

A.4. Map Understanding and Navigation

The ability to "read" a map as a semantic document is distinct from visual matching. Benchmarks such as **MapQA** (Li et al., 2025) and **MAPWise** (Mukhopadhyay et al., 2025) evaluate VLMs on their ability to ground text labels and reason about topological relationships in cartographic data. In the context of embodied AI, the **Touchdown** benchmark (Chen et al., 2019) tasks agents with navigating Street View environments based on natural language instructions, focusing on sequential language grounding. **m2sv** complements these by isolating the *single-step geometric alignment primitive* between egocentric and allocentric views. Unlike cartographic literacy benchmarks like **MapQA** or diagram-reasoning tasks like **MathVista** (Lu et al., 2024), **m2sv** specifically tests topology understanding through the lens of orientation in real-world environments.

A.5. Benchmark Theory and Saturation

The rapid progress of VLMs has led to the saturation of traditional benchmarks like MMLU and GSM8K (Stanford HAI, 2024; Ott et al., 2022). This has created an urgent need for "unsaturated" tests that remain challenging for frontier models. New benchmarks like **FrontierMath** (Glazer et al., 2024) and **DynaMath** (Zou et al., 2025) prioritize multi-step reasoning and dynamic variations to prevent memorization. **m2sv** fits this paradigm by requiring geometric alignment between two real-world inputs, making it resistant to pattern-matching shortcuts and data contamination. The large gap between human performance (95%) and current model accuracy (65%) confirms its utility as a diagnostic for future progress in grounded spatial reasoning.

Table 5. MindCube evaluation suite with varying input/output formats.

Input	Output Format	Base	SFT	SFT+RL
Raw + q	Aug + rsn → ans	34.5	34.0	33.2
Aug. + QA	Direct answer	24.6	37.6	41.0
Aug. + QA	Rsn → answer	46.9	40.3	46.1
Raw + q	Rsn → answer	38.5	36.8	36.6
Raw + q	Map + rsn → ans	34.7	33.5	35.2
Raw + q	Direct answer	27.0	34.9	34.7



Ground truth: A, Prediction: C

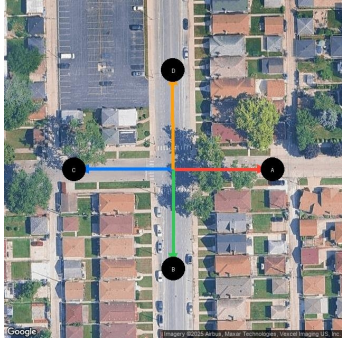
Model trace (excerpt):

Direction A: This arrow points east-southeast down a relatively narrow residential street. It has no crosswalks visible across its width.

Direction C: This arrow points west-northwest down a much wider road than A and B. This main road clearly has multiple lanes separated by what appear to be painted lines, indicating it's a major thoroughfare. Crosswalks are visible crossing this road.

Failure: A and C are two sides of the same street so the road width is the same, but the answer emphasizes the road width as the key factor

(a) Failure to maintain a consistent spatial representation



Ground truth: D, Prediction: C

Model trace (excerpt):

Option D: This view looks up the main, wide road. On the northeast corner (on the right), there is a residential house. On the northwest corner (on the left), there is the commercial building. This arrangement is the opposite of what is seen in the street view photo, where the commercial building is on the left and the house is on the right.

Failure: The model correctly identifies left-right relationships but subsequently contradicts its own assignments, losing track of spatial state during verbalization.

(b) Internal contradiction and state inconsistency



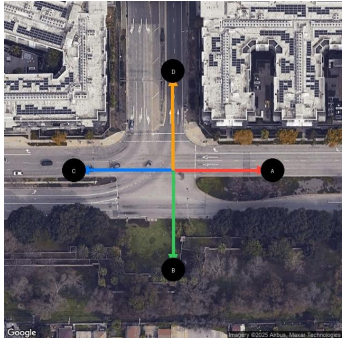
Ground truth: D, Prediction: B

Model trace (excerpt):

For view B: Left = Building A, Right = Long Rectangular Building. For view D: Left = Large Building with Parking Lot, Right = Building A. Comparing the photo to view B: We see a specific yellowish building on the left and a gas station on the right.

Failure: The model correctly narrows the decision to two symmetric candidates (B and D), but fails to use subtle geometric cues—such as building orientation relative to the road—to break symmetry, instead introducing unsupported semantic evidence (e.g., a gas station).

(c) Symmetry traps and insufficient cue escalation.



Ground truth: D, Prediction: A

Model trace (excerpt):

Direction A provides the most complete match. It correctly places large buildings on both sides of the road and crucially includes the distant underpass/bridge structure that is clearly visible in the street view photo.

Failure: The model invents or misattributes a nonexistent large-scale structure (underpass/bridge) and then reasons as if it were present in the map.

(d) False landmark projection

Figure 8. More qualitative failure modes on m2sv. Each row shows the same map–street-view pair with a different erroneous reasoning pattern exhibited by the model. From left to right: overhead map with candidate directions, corresponding street-view image, and an excerpt from the model’s reasoning trace highlighting the incorrect assumption. All examples are correctly solved by human annotators.